Title

Imaging versus electrographic connectivity in human mood-related fronto-temporal networks

Journal

Brain Stimulation, 15(3)

ISSN

1935-861X

Authors

Adkinson, Joshua A
Tsolaki, Evangelia
Sheth, Sameer A
et al.

Publication Date

2022-05-01

DOI

10.1016/j.brs.2022.03.002

HHS Public Access

Author manuscript

Brain Stimul. Author manuscript; available in PMC 2023 May 01.

Published in final edited form as:

Brain Stimul. 2022 ; 15(3): 554–565. doi:10.1016/j.brs.2022.03.002.

Corresponding Author: Kelly R. Bijanki, Ph.D., S101D Smith Biomedical Research Building, One Baylor Plaza, Houston, TX 77030. bijanki@bcm.edu. Phone: 713-798-1353.

*authors contributed equally to the work

†authors contributed equally to the work

Credit Author Statement:

Joshua Adkinson: conceptualization, methodology, software, validation, formal analysis, writing original draft, visualization. Evangelia Tsolaki: conceptualization, methodology, software, validation, formal analysis, writing original draft, visualization. Sameer Sheth: conceptualization, methodology, writing – review and editing, supervision, funding acquisition. Denise Oswalt: methodology, software, investigation, formal analysis, writing – review and editing. Brian Metzger: methodology, validation, resources, writing – reviewing and editing. Cameron C. McIntyre: methodology, visualization, writing – reviewing and editing. Raissa K. Mathura: methodology, resources, data curation, project administration, writing – reviewing and editing, visualization, Allison C. Waters: conceptualization, visualization, writing – reviewing and editing. Meghan E. Robinson: methodology, validation, resources, data curation, writing – review and editing. Anusha B. Allawala: methodology, software, resources, data curation, writing – review and editing. Angela M. Noecker: methodology, visualization, writing – review and editing, Mahsa Malekmohammadi: methodology, visualization, writing – review and editing, Kevin Chiu: methodology, visualization, writing – review and editing, Richard Mustakos: methodology, visualization, writing – review and editing, Wayne Goodman: writing – review and editing, supervision, funding acquisition. David Borton: methodology, writing – review and editing. Nader Pouratian: conceptualization, methodology, validation, formal analysis, writing -review and editing, visualization, funding acquisition. Kelly R. Bijanki: conceptualization, methodology, validation, formal analysis, writing original draft, visualization, writing – reviewing and editing, supervision, project administration.

Author Contributions:

KRB, SAS, JAA conceived of the study, all co-authors participated in review of analyses and development of the narrative. KRB, JAA, DO, ACW, CCM, NP, and SAS designed the approach for pulse-evoked potentials. MER collected the neuroimaging data. KRB, JAA, ABA, BAM, and DO collected the pulse-evoked potentials data. JAA and KRB conducted the evoked potentials analysis. ET, AMN, CCM, and NP conducted the tractography analysis, KRB, JAA, and ET wrote the manuscript, all co-authors revised the manuscript. MM, KC, and RM calculated the stimulation field volumes. SAS, NP, and WG obtained funding for the study.

Disclosures

CCM is a paid consultant for Boston Scientific Neuromodulation, receives royalties from Hologram Consultants, Neuros Medical, Qr8 Health, and is a shareholder in the following companies: Hologram Consultants, Surgical Information Sciences, CereGate, Autonomic Technologies, Cardionomic, Enspire DBS. NP is a consultant for Abbott. SAS is a consultant for Boston Scientific, Zimmer Biomet, Neuropace, Abbott, and Koh Young. MM and RM are employees of Boston Scientific Corporation. KC is a paid full-time employee of Brainlab, Inc. JAA, ET, DO, BAM, RKM, ACW, MER, ABA, AMN, WG, DB, and KRB do not report biomedical financial interests or potential conflicts of interest.

Declaration of Interests

We wish to draw the attention of the Editor to the following facts which may be considered as potential conflicts of interest and to significant financial contributions to this work.

The following authors make the following disclosures:

• Cameron C. McIntyre is a paid consultant for Boston Scientific Neuromodulation, receives royalties from Hologram Consultants, Neuros Medical, Qr8 Health, and is a shareholder in the following companies: Hologram Consultants, Surgical Information Sciences, CereGate, Autonomic Technologies, Cardionomic, Enspire DBS.
• Nader Pouratian is a consultant for Abbott.
• Sameer A. Sheth is a consultant for Boston Scientific, Zimmer Biomet, Neuropace, Abbott, and Koh Young.
• Mahsa Malekmohammadi and Richard Mustakos are employees of Boston Scientific Corporation.
• Kevin Chiu is a paid full-time employee of Brainlab, Inc.

The following authors do not report biomedical financial interests or potential conflicts of interest:

• Joshua A. Adkinson
• Evangelia Tsolaki
• Denise Oswalt
• Brian A. Metzger
• Raissa K. Mathura
• Allison C. Waters
• Meghan E. Robinson
• Anusha B. Allawala
• Angela M. Noecker
• Wayne Goodman
• David Borton
• Kelly R. Bijanki

We confirm that the manuscript has been read and approved by all named authors and that there are no other persons who satisfied the criteria for authorship but are not listed. We further confirm that the order of authors listed in the manuscript has been approved by all of us.

We confirm that we have given due consideration to the protection of intellectual property associated with this work and that there are no impediments to publication, including the timing of publication, with respect to intellectual property. In so doing we confirm that we have followed the regulations of our institutions concerning intellectual property.

Imaging versus electrographic connectivity in human mood-related fronto-temporal networks

Joshua A. Adkinson[*,a],
Evangelia Tsolaki[*,b],
Sameer A. Sheth[a],
Brian A. Metzger[a],
Meghan E. Robinson[a],
Denise Oswalt[a],
Cameron C. McIntyre[c],
Raissa K. Mathura[a],
Allison C. Waters[d],
Anusha B. Allawala[e],
Angela M. Noecker[c],
Mahsa Malekmohammadi[i],
Kevin Chiu[j],
Richard Mustakos[i],
Wayne Goodman[f],
David Borton[e,g],
Nader Pouratian[†,h],
Kelly R. Bijanki[†,a]

[a]Department of Neurosurgery, Baylor College of Medicine, One Baylor Plaza, Houston, TX 77030, USA

[b]Department of Neurosurgery, David Geffen School of Medicine at UCLA, 300 Stein Plaza Suite 562, Los Angeles, CA 90095, USA

[c]Department of Biomedical Engineering, Case Western Reserve University, 10900 Euclid Ave., Cleveland, OH 44106, USA.

[d]Department of Psychiatry, Mount Sinai School of Medicine, 1000 10th Ave., New York, NY 10019, USA

We further confirm that any aspect of the work covered in this manuscript that has involved either experimental animals or human patients has been conducted with the ethical approval of all relevant bodies and that such approvals are acknowledged within the manuscript.

We understand that the Corresponding Author is the sole contact for the Editorial process (including Editorial Manager and direct communications with the office). He/she is responsible for communicating with the other authors about progress, submissions of revisions and final approval of proofs. We confirm that we have provided a current, correct email address which is accessible by the Corresponding Author and which has been configured to accept email from Kelly.Bijanki@bcm.edu

[e]School of Engineering, Brown University, 182 Hope St., Providence, RI 02912 USA.

[f]Department of Psychiatry and Behavioral Sciences, Baylor College of Medicine, 1977 Butler Blvd., Houston, TX 77030, USA

[g]Center for Neurorestoration and Neurotechnology, Rehabilitation R&D Service, Department of Veterans Affairs, Providence, RI 02912 USA.

[h]Department of Neurological Surgery, University of Texas Southwestern Medical Center, 8353 Harry Hines Blvd MC8855, Dallas, TX 75239, USA.

[i]Boston Scientific Neuromodulation, 25155 Rye Canyon Loop, Valencia, CA, 91355, USA.

[j]Brainlab, Inc., 5 Westbrook Corporate Center, Suite 1000, Westchester IL 60154, USA.

Structured Abstract

Background: The efficacy of psychiatric DBS is thought to be driven by the connectivity of stimulation targets with mood-relevant fronto-temporal networks, which is typically evaluated using diffusion-weighted tractography.

Objective: Leverage intracranial electrophysiology recordings to better predict the circuit-wide effects of neuromodulation to white matter targets. We hypothesize strong convergence between tractography-predicted structural connectivity and stimulation-induced electrophysiological responses.

Methods: Evoked potentials were elicited by single-pulse stimulation to two common DBS targets for treatment-resistant depression – the subcallosal cingulate (SCC) and ventral capsule/ventral striatum (VCVS) – in two patients undergoing DBS with stereo-electroencephalographic (sEEG) monitoring. Evoked potentials were compared with predicted structural connectivity between DBS leads and sEEG contacts using probabilistic, patient-specific diffusion-weighted tractography.

Results: Evoked potentials and tractography showed strong convergence in both patients in orbitofrontal, ventromedial prefrontal, and lateral prefrontal cortices for both SCC and VCVS stimulation targets. Low convergence was found in anterior cingulate (ACC), where tractography predicted structural connectivity from SCC targets but produced no evoked potentials during SCC stimulation. Further, tractography predicted no connectivity to ACC from VCVS targets, but VCVS stimulation produced robust evoked potentials.

Conclusion: The two connectivity methods showed significant convergence, but important differences emerged with respect to the ability of tractography to predict electrophysiological connectivity between SCC and VCVS to regions of the mood-related network. This multimodal approach raises intriguing implications for the use of tractography in surgical targeting and provides new data to enhance our understanding of the network-wide effects of neuromodulation.

Keywords

Tractography; Diffusion; DBS; Evoked Potentials; Connectivity; Cortico-cortical

Introduction

After decades of research and clinical implementation, the therapeutic mechanism of deep brain stimulation (DBS) remains incompletely understood. It is hypothesized that DBS modulates local activity near the stimulating electrode and drives network-wide changes in neural activity mediated by stimulated white matter systems [1]–[3]. Effective treatment of psychiatric diseases likely relies on the engagement of multiple nodes of a connected network [4]. Perhaps it is no surprise that the leading DBS targets for psychiatric indications tend to be confluences of white matter fiber systems. Delineating functionally relevant fiber pathways underlying psychiatric diseases is a critical goal for basic science as well as for developing new targets. Enhanced understanding of these fiber pathways will impact preoperative patient evaluation, intervention planning, surgical targeting and intraoperative navigation [5].

Two white matter hubs have risen to prominence as neuromodulation targets for psychiatric disorders, particularly treatment-resistant depression (TRD): the ventral capsule/ventral striatum (VCVS) and the subcallosal cingulate (SCC) [6], [7], [16], [17], [8]–[15]. The VCVS target contains fibers connecting the dorsal prefrontal cortex, orbitofrontal cortex and ventromedial prefrontal cortex with thalamus, amygdala, hypothalamus and brainstem [18], [19]. The SCC target contains fibers connecting to medial frontal cortex through the bilateral forceps minor of the anterior corpus callosum, to anterior and posterior cingulate through cingulum bundles and to medial frontal cortex rostrally and to nucleus accumbens, anterior thalamus and other subcortical regions through the medial branch of the uncinate fasciculus [18], [20]. The connectivity of these targets have been well studied with diffusion-weighted imaging (DWI) [3], [19], [21]–[25].

DWI is a neuroimaging modality used to study structural connectivity and white matter properties of the living human brain [2], [3], [5], [12], [26]–[29]. Despite technological and analytic advances, knowledge gaps remain regarding the extent of DWI-based tractography for providing accurate maps of brain connections and the homogeneity of this technique across brain regions [30]–[32]. Available tractography algorithms have achieved at best modest degrees of convergence with histological tracer studies, the gold standard for precisely identifying connections between brain areas in primate models with high spatial accuracy [33]–[35]. Moreover, electrophysiological validation of MR-based tractography remains sparse in general, and nearly absent for the SCC and VCVS targets [36].

In this study, we leverage a unique opportunity in two human research participants implanted simultaneously with DBS leads in SCC and VCVS and stereo-EEG (sEEG) electrodes across the frontal-temporal mood network to evaluate tractography-based connectivity predictions. We apply single pulses of intracranial neural stimulation to the SCC and VCVS, a technique which is understood to generate axonal depolarization and trigger action potentials to propagate through the affected circuitry [37], [38], resulting in neurotransmission events in the cortex. This technique allows us to investigate structural connections to mood-related brain networks but also compare these findings to DWI-based tractography measurements to determine the degree of convergence between these two modalities.

Methods and Materials

Participant and study overview:

This study reports data from two subjects (37 year old Latino man, 56 year old Caucasian woman) diagnosed with recurrent major depressive disorder without psychotic features. Participant 2 has a history of migraines. Both are participants in an ongoing clinical trial (NCT 03437928) aimed at using a novel platform for DBS therapy development based on elucidating the electrophysiological mechanisms underlying DBS for TRD [39]. The subjects provided written informed consent as approved by the Baylor College of Medicine IRB (H-43036) prior to participation. Subjects underwent stereotactic implantation of four segmented DBS leads (Boston Scientific Cartesia; Figure 1a) and 10 temporary sEEG electrodes (PMT) (Figure 1b) based on pre-operative patient-specific tractography. Following implantation, and per study protocol, the patients underwent a ten-day intracranial monitoring period to better understand brain networks involved in treatment refractory major depressive disorder. After the intracranial monitoring period, sEEG electrodes were removed and the two DBS systems were internalized and connected to two implanted pulse generators (Boston Scientific Gevia).

Neuroimaging:

T1-weighted anatomical imaging (MPRAGE; TR/TE/TI=2400/2.24/1160; FOV=256; 208 slices; flip angle=8°) and DWI were acquired for both participants prior to surgical implantation of DBS and sEEG electrodes. High-resolution DWI data were acquired (1.5mm isotropic) with two phase encode directions (anterior-to-posterior and posterior-to-anterior), 92 diffusion-sensitizing gradient directions, and 7 interleaved b=0 volumes. The diffusion-encoded volumes alternated between b=2000 and b=1000, with TR=3.2s, TE=87ms, TA=5:34 per scan, matrix 140×140×92, multi-slice acceleration=4 on a Siemens Prisma 3T scanner. Post-implantation clinical CT scans were acquired on a Philips iCT 256 system, using a reconstruction diameter of 250mm, slice thickness of 0.67mm and a space between slices of 0.67mm, image size = 512×512, view size 1664×1236.

Electrode implantation layout:

DBS leads were implanted bilaterally in the VCVS and SCC. These targets lie at the intersections of several white matter pathways connecting brain regions related to depressive symptoms [40]. Corresponding sEEG contacts were implanted bilaterally to target the gray matter regions believed to be connected to these DBS targets via white matter projections. These targets include the dorso-lateral prefrontal cortex (dlPFC), ventro-lateral and ventro-medial prefrontal cortex (vlPFC, vmPFC), medial and lateral orbitofrontal cortex (mOFC and lOFC), anterior cingulate cortex (ACC), and amygdala [41], [42]. Contacts near the skull or within the surgical bolt were identified and excluded from analysis. Electrode contacts were labeled by broad regions of interest (Figures 3 and 4) based on automatic cortical reconstruction using FreeSurfer (http://surfer.nmr.mgh.harvard.edu) [43]. Postoperative CT and preoperative MRI were aligned using the Functional Magnetic Resonance Imaging for the Brain Software Library's (FMRIB's) Linear Image Registration Tool (FLIRT) [44], [45]. Electrode coordinates were manually determined from the co-registered CT in BioImage Suite [46] and placed into native MRI space. The regions of

interest were determined by visual inspection of the contacts plotted on each brain slice by an expert rater, including mOFC, lOFC, VPFC - including ventromedial and ventrolateral prefrontal positions, DPFC - including dorsomedial and dorsolateral prefrontal positions, ACC, amygdala, and the middle and superior temporal gyri (MTG, STG). The reconstructed cortical surface, segmented subcortical structures, and electrode coordinates were visualized using RAVE [47]. Anatomical locations of each sEEG contact are presented (Supplementary Material S2, S3, and S4).

Modeling of stimulation fields and sEEG recording locations:

Boston Scientific Cartesia DBS leads feature eight stimulation contacts: solid ring electrodes at the deepest and shallowest positions and three-way segmented contacts at the middle two electrode positions (Figure 1A). Twenty stimulation configurations were tested: Five configurations were tested per each of four leads, including: (1) the deepest contact (contact 1); (2) the monopolar stack of segmented contacts facing anteriorly (contacts 2 and 5); (3) the monopolar stack of contacts facing posterior-right (contacts 3 and 6); (4) the monopolar stack of segmented contacts facing posterior-left (contacts 4 and 7); and (5) the shallowest contact (contact 8).

To generate the stimulation field model (SFM) for a given stimulation experiment, electric fields resulting from respective stimulation settings were modeled using COMSOL Multiphysics software (COMSOL Inc., Burlington, MA, USA) and transformed for inclusion into GuideXT (Boston Scientific Neuromodulation, Valencia, CA, USA). The parameters for a given DBS electric field had identical polarity, pulse width, amplitude, and contact configuration to those applied during the stimulation experiments. Super-position was used to create each fractionalization-specific voltage field, and the resulting electric field potential as a grid of finite elements is applied to an approximator trained to model an axon activation threshold (5.7μm diameter, MRG model [48]). These current amplitude thresholds are then iso-surfaced at the selected stimulation current amplitude, and the resulting surface is displayed as the SFM. Exemplar SFM shown as red manifold in Figure 1A.

SFM masks were registered to diffusion space using linear registration (FLIRT) [45]. On the postoperative CT we used each sEEG contact coordinate as a center point, creating a spherical mask for each contact and then registering to diffusion space using FLIRT.

Patient-specific Tractography:

Data from two phase encode directions were combined and susceptibility-induced distortion was estimated using Topup (FSL v.6.0.3) [49]. Movement and current-induced distortions were corrected using Eddy (FSL v.6.0.3) [50]. A multi-fiber diffusion model was fit (FDT) [51], using Bayesian techniques to account for the possibility of crossing fibers. Two fiber directions were modeled per voxel, using a multiplicative factor of 1, and 1000 iterations before sampling. Diffusion and T1 data were skull stripped using the FSL Brain Extraction Tool [52]. The T1 image was segmented [53] to create a cerebrospinal fluid (CSF) mask used later to restrict tractography results to brain voxels only, and linearly registered to diffusion space.

Streamline analysis:

Structural connectivity was calculated as the number of streamlines between different DBS stimulation configurations and sEEG recording contacts. SFMs were utilized as the seed region for whole-brain probabilistic diffusion-weighted tractography in diffusion space [54], (samples=5000, curvature threshold=0.2, loopcheck termination, 2000 maximum steps, step length=0.5mm, subsidiary fiber fraction threshold=0.01), using a whole-brain target and CSF as an exclusion mask. Using a spherical target mask of 10mm radius centered on each sEEG contact location, the number of streamlines intersecting each sEEG contact was enumerated (Supplementary Methods and Figure S1). For each volume of joint intersection (SFM to sEEG), the number of voxels and the mean value of streamlines were derived using the "fslstats" tool in FSL. A visual example of this streamline analysis is illustrated in Figure 2 panel A, C, and E.

Single-Pulse Stimulation and Electrophysiology Recording:

Monopolar cathodic single pulse stimulation was delivered via a Blackrock CereStim R96 (Blackrock Microsystems, Utah) to the patient as well as via analog input directly into the recording system for temporal alignment. Stimulation amplitudes were 5mA in Patient A and 4.8mA in Patient B. Both patients' stimulation used a pulse width of 180μs, a 100μs interphase gap. Twenty stimulation experiments examined five distinct electrode configurations on each of four DBS leads. Stimulation experiments included 315 stimulation pulses each, delivered every 600ms with a uniformly random jitter ranging from 1ms to 200ms. All stimulation experiments were performed with the patients awake. Electrophysiological signals from implanted sEEG contacts were recorded using a Blackrock Microsystems NeuroPort Acquisition System. Signals were amplified then sampled with a 2kHz (Patient A) or 30kHz (Patient B) sampling rate.

Evoked Potentials Analysis:

For all signal-based data analysis and statistical analyses, custom scripts were written in MATLAB 2019b (http://github.com/adkinson/PEP). Prior to analysis, channels were removed from the dataset if they were found to contain excessive artifactual noise determined by visual inspection of each contact's power spectrum. Laplacian re-referencing was applied to the sEEG data [55]. Individual stimulation trials were epoched with respect to the stimulation pulse onset.

Based on visual inspection of the data, the evoked potential analysis window was defined as 10ms to 150ms after stimulation pulse onset in order to exclude stimulation artifact and amplifier desaturation. For each stimulation experiment, an average waveform for each sEEG contact was calculated by averaging across all 315 stimulation trials. To determine if the average waveform at each sEEG contact represented an evoked response, the following thresholding technique was employed: (1) calculate the standard deviation of the trial-averaged waveform per contact across time, σ_{Orig}; (2) randomly shuffle each trial used to generate the original average waveform across its time domain (within the 10ms-150ms analysis window); (3) average across these shuffled trials to generate a surrogate trial-averaged waveform per contact; (4) calculate the standard deviation of this trial-averaged surrogate waveform across time, σ_{Surr}; (5) sEEG contacts have a potentially

substantial evoked response to the stimulation if $\sigma_{Orig} > p\sigma_{Surr}$. We chose a value of $p = 3$ as an intentionally conservative threshold. To mitigate false positives arising via the shuffling process, this thresholding technique was repeated one thousand times, and sEEG contacts that satisfied the thresholding criterion at least 95% of the time were classified as having an evoked response from the given stimulation configuration. A visual example of evoked potentials analysis is illustrated in Figure 2 panel B, D, and F. Representative waveforms are presented in Figure 2 panel G showing evoked potentials from MOFC and VPFC as well recordings from locations without evoked potentials from LOFC and DPFC. Two of the traces represent stimulation evoked responses and two show no activity at contacts not responding to stimulation.

Multimodal analysis:

We investigated the relationship between streamlines and evoked potentials using two methods: (1) point-biserial correlation, and (2) receiver operating characteristic (ROC) curves. In each method, streamline counts for each sEEG contact were treated as a continuous variable and evoked potentials were quantified as a dichotomous variable in which an evoked response either did or did not occur at each sEEG contact.

Point-biserial correlation, a special case of Pearson's correlation, measures the relationship between two random variables when one of the random variables is continuous and the other is dichotomous. Let X be the streamline counts for all contacts and stimulation experiments and Y is the presence (Y=1) or absence (Y=0) of an ERP response across the same space. If $X_{Y=0}$ is the subset of streamline counts where the corresponding contact/stimulation experiment did not show an ERP response, and $X_{Y=1}$ is the subset of streamline counts with a respective ERP response, then the point-biserial correlation r_{pb} is defined as $r_{pd} = \frac{\mu(X_Y = 1) - \mu(X_Y = 0)}{\sigma(X)}\sqrt{\frac{n_Y = 1 n_Y = 0}{n^2}}$, where the functions $\mu(\cdot)$ and $\sigma(\cdot)$ are the mean and standard deviation of the given inputs, respectively, and n is the number of elements in Y for the specified subset of Y.

ROC curves illustrate the efficacy of streamline counts to classify evoked potential occurrences across sEEG contacts. True positive rates (TPR) and false positive rates (FPR) were calculated by thresholding the streamline counts and comparing to the occurrence of evoked potentials; all possible thresholds of streamline counts were considered to generate the full ROC curve. The area under the curve (AUC) for each ROC curve was calculated as a measure of the effectiveness of each target volume level for classifying the evoked potential occurrences. AUC's and their respective confidence intervals were estimated using the R package pROC [56]; confidence intervals were estimated using Delong's method [57]. To calculate a p-value for a given AUC, we performed a Monte Carlo estimation where we randomly permute the association between evoked responses and streamline counts and estimated that random AUC. This process was replicated 100,000 times to create a distribution of random AUCs. The p-value was calculated as $p_{MC} = \frac{r + 1}{n + 1}$, where r is the number of random AUCs which are greater than the original AUC and n is the total number of replicates of this test [58]. These calculations were made separately for each participant, as well as by each stimulation target (VCVS and SCC).

Due to the potential for shared noise among sEEG contacts to result in correlated observation errors, the significance of the correlation estimation may be inflated. However, the degree of that inflation is unknown, as nearby contacts are also likely to be functionally similar and may be correlated because of true similarity. Thus, we performed Monte Carlo permutation testing of the point-biserial correlation between the two datasets using 8 different permutation strategies to modeled the shared variance. For each patient, the permutation strategy that provided the most conservative p-value was treated as a "empirically-corrected" p-value. Details of the permutation strategies employed and the derived Monte Carlo distributions can be found in the Results section as well as the Supplementary Methods and Supplementary Figures S4, S5, S6, and S7.

A further analysis was undertaken to protect against the risk of correlated observation errors. A linear mixed effects model was calculated for each patient. The model consisted of two fixed effects: (1) the logarithm of streamline counts and (2) the Euclidean distance between a DBS contact and a respective sEEG contact. The random effects were (1) the logarithm of streamline counts, (2) a categorical variable indicating which lead was the source of a given stimulation, and (3) a categorical variable indicating which SFM on a given lead was the source of a given stimulation. Estimated beta weights of the fixed effects and their associated p-values were considered. Estimation of the model was performed in R using the lme4 package.

Results

Comparison between DWI tractography and stimulation-evoked potentials reveals similar patterns of connectivity in two patients (Patient A: Figure 3; Patient B: Figure 4). In both patients, SCC stimulation tends to produce bilateral engagement, both in terms of tractography and in evoked potentials. By contrast, VCVS stimulation produces unilateral predicted structural connectivity via tractography and more ipsilateral evoked potentials. We examined the findings of the two connectivity indices by mood-relevant regions of interest.

Orbitofrontal cortex:

SCC tractography predicts bilateral engagement of the medial orbitofrontal cortex in both patients (Figure 3A, Figure 4A). VCVS tractography predicts engagement of adjacent but more lateral and superior fiber tracks of the medial orbitofrontal cortex, and only on contacts ipsilateral to the stimulation volume (Figure 3A, Figure 4A). Similar patterns occur in the evoked potentials: SCC stimulation elicits evoked potentials in the medial OFC bilaterally (Figure 3B, Figure 4B), whereas VCVS stimulation elicits evoked potentials in the adjacent lateral OFC contacts (Figure 3B, Figure 4B) ipsilateral to stimulation. Similar patterns are observed with respect to the lateral OFC region of interest: SCC tractography predicts bilateral innervation and VCVS tractography predicts ipsilateral innervation. Lateral OFC evoked potentials are more sparse than those in the medial OFC region of interest, with possible exception of the right VCVS producing ipsilateral evoked potentials in lateral OFC. Overall, evoked potentials tend to be elicited more robustly from current directions 1 and 8 (solid non-segmented contacts at the inferior-most and superior-most position on the DBS

lead), and somewhat less robustly elicited from the segmented contact stacks (2–5, 3–6, or 4–7) despite identical charge injection.

Anterior cingulate:

Tractography predicts strong engagement of the ACC from SCC SFMs, and negligible engagement of the ACC from VCVS SFMs in both patients. These streamlines are predominantly ipsilateral to the SCC stimulation site (Figure 3A, Figure 4A). Evoked potentials reveal the opposite pattern. In both patients we observe very weak evoked potentials from SCC stimulation, and unexpectedly robust responses from VCVS stimulation. These evoked potentials are recorded in the anterior cingulate contacts with left VCVS stimulation, and to a lesser extent with right VCVS stimulation (Figure 3B, Figure 4B). This finding represents an area engaged by VCVS stimulation not previously understood from tractography predictions and anatomical study of the anterior limb of the internal capsule.

Ventromedial prefrontal cortex:

SCC tractography analysis shows strong bilateral predicted engagement of the medial wall of the ventral prefrontal cortex in both patients (Figure 3A, Figure 4A). VCVS stimulation volumes produce engagement of more dorsal white matter fibers of the prefrontal cortex (Figure 3A, Figure 4A), and only ipsilateral to stimulation. This pattern is recapitulated in the evoked potential analysis with SCC stimulations eliciting evoked potentials from bilateral gray matter contacts in the medial wall of the VPFC (Figure 3B, Figure 4B). One divergent pattern is observed with tractography predicting VPFC engagement by ipsilateral VCVS stimulation in superjacent white matter contacts, whereas evoked potentials are recorded on contacts in the ventral-most position on the sEEG electrode, corresponding to gray matter of the medial wall of the VPFC.

Amygdala:

Both VCVS and SCC tractography analysis show predicted streamlines to amygdala exclusively from ipsilateral stimulation sites. These analyses demonstrate white matter contacts corresponding to the uncinate fasciculus to be engaged by VCVS stimulation (Figure 3A, Figure 4A), whereas evoked potential analysis reveals responses from the gray matter of the amygdala proper (Figure 3B, Figure 4B).

Multimodal data integration analysis:

For patient A, the calculated point-biserial correlation between the streamlines and the evoked potential occurrences was $r_{pb} = 0.4185$ with a p-value derived Student's t-test of $p = 1.7584 \times 10^{-112}$. Patient B showed a point-biserial correlation value of $r_{pb} = 0.3486$ with a p-value of $p = 4.9408 \times 10^{-110}$. Because of the risk of correlated observation errors contributing to an inflated estimate of significance, we calculated a series of p-values from Monte Carlo permutation schemes that modeled the shared noise. Both patients showed statistically significant correlations between streamline counts and evoked potentials for all permutation strategies. For both patients, all permutation schemes reached significance of $p_{MC} < 0.05$. Most strategies for both patients estimated p-values of $p_{MC} = 9.99 \times 10^{-6}$. One

strategy gave a p-value of $p_{MC} = 1.71 \times 10^{-3}$ for Patient A and $p_{MC} = 2.10 \times 10^{-4}$ for Patient B, and another, which was constrained by a low number of possible permutations, gave corrected p-values of $p_{MC} = 0.04156$ for Patient A and $p_{MC} = 0.0413$ for Patient B. See all simulated distributions for both patients in Supplementary Figures S4 and S5.

For the linear mixed effects model, Patient A shows a beta weight for the logarithm of streamline counts fixed effect of $\beta = 0.448 \pm 0.109$ with a p-value of $p = 4.08 \times 10^{-5}$ and the effect of the distance from DBS contacts to sEEG contacts is $\beta = -0.0753 \pm 0.0775$ with a p-value of $p = 2.0 \times 10^{-16}$. For Patient B, the estimated effect from the logarithm of streamline counts is $\beta = 0.206 \pm 0.0521$ with a p-value of $p = 7.82 \times 10^{-5}$ and the effect of the distance from DBS contacts to sEEG contacts is $\beta = -0.0813 \pm 0.0665$ with a p-value of $p = 2.0 \times 10^{-16}$. Note that the inclusion of the logarithm of streamline counts resulted in a near singular model for both patients, but removal of this random effect from the model nullifies that singularity.

ROC curves were created for each patient to quantify the extent to which the streamlines data can predict evoked potential occurrence across all stimulation experiments (Figure 5A). Using a 95% confidence interval, AUCs for these ROC curves (Patient A: $AUC = 0.7956 \pm 0.0241$; Patient B: $AUC = 0.7129 \pm 0.0258$) support the hypothesis that streamlines classify the evoked potentials better than random chance. The strength of this predictive relationship was then examined separately for each DBS target (VCVS and SCC) (Figure 5B). Both patients show stronger relationships between the streamlines and evoked potentials for SCC stimulation than VCVS (Patient A: $AUC_{SCC} = 0.8727 \pm 0.0266$, Patient B: $AUC_{SCC} = 0.8407 \pm 0.0293$, Patient A: $AUC_{VCVS} = 0.7702 \pm 0.0343$, Patient B: $AUC_{VCVS} = 0.6577 \pm 0.036$). Delong's test for comparing two ROC curves was also performed, comparing the SCC and VCVS ROC curves in each patient. For patient A, Delong's test provides a p-value of $p = 3.876 \times 10^{-6}$, and for patient B, Delong's test estimates a p-value of $p = 1.49 \times 10^{-14}$. Both cases would reject the null hypothesis that the AUCs are equivalent. However, note these within-patient comparisons between SCC and VCVS curves are non-paired ROC curve comparison tests because contacts generating evoked potentials were not identical between SCC and VCVS stimulation.

Lastly, p-values were calculated via Monte Carlo estimation to determine if each AUCs for each ROC were different from AUCs from randomly shuffled data. For each ROC curve, p-values indicate that the AUCs are different from random AUCs (Patient A: $p_{All} = 1.0 \times 10^{-5}$, $p_{SCC} = 1.0 \times 10^{-5}$, $p_{VCVS} = 1.0 \times 10^{-5}$; Patient B: $p_{All} = 1.0 \times 10^{-5}$, $p_{SCC} = 1.0 \times 10^{-5}$, $p_{VCVS} = 1.0 \times 10^{-5}$). These Monte Carlo distributions have been added as Supplementary S8.

Discussion

The findings of this study demonstrate substantial convergence between two methods of quantifying connectivity, while revealing important differences between them. These results help identify putative networks involved when stimulating the subcallosal cingulate and ventral capsule/ventral striatum, two important hubs mediating antidepressant response in DBS trials for treatment-resistant depression. Both connectivity metrics (streamlines

and evoked potentials) suggest that SCC stimulation produces bilateral engagement of prefrontal affective networks while VCVS stimulation predominantly engages unilateral structures. For SCC stimulation, streamline and evoked potentials analyses are largely convergent, with both metrics demonstrating bilateral engagement of the medial and lateral orbitofrontal cortex and the ventromedial prefrontal cortex. SCC stimulation volumes tend to produce robust streamlines indicating connectivity with the anterior cingulate cortex, but evoked potentials following SCC stimulation were notably absent. For VCVS stimulation, streamline and evoked potentials analyses were less convergent than SCC stimulation analysis. Both connectivity metrics show VCVS stimulation engaging the ipsilateral orbitofrontal cortex, ventromedial prefrontal cortex, and amygdala. In the orbitofrontal cortex, VCVS stimulation produced engagement in positions slightly more lateral than those activated with SCC stimulation.

Notable divergence between streamline and evoked potentials analysis is observed in the dorsal anterior cingulate. SCC streamlines indicate robust engagement of the ACC, most likely mediated by the cingulum bundle [3], [20], but virtually no evoked potentials are detected within dorsal ACC. Meanwhile, VCVS streamlines indicate no fiber tracks projecting to the anterior cingulate, but robust evoked potentials arise from stimulation to the VCVS. This double dissociation has interesting implications for our understanding of the prefrontal networks modulated in DBS. Single pulse stimulation can give rise to both orthodromic and antidromic action potential propagation and drive the firing of neural assemblies from polysynaptic innervation through modulated networks that may not be adequately reflected in the streamline data. To our knowledge, this study presents novel evidence of the dorsal ACC being involved in VCVS stimulation. These findings underscore the need for a deeper understanding of both connectivity modalities. An in-depth histological study of the anterior cingulate anatomy and its responsiveness to DBS stimulation would greatly benefit this need. The networks making up the complex prefrontal circuity examined in this study are only beginning to be defined and will be aided by bringing to bear considerations of anterograde and retrograde propagation patterns as a function of detailed characterization of the anatomy from histological tracer studies and integration of insights gained from animal connectivity studies. This multimodal analysis provides an important step in expanding our understanding of those networks.

Increasingly advanced neuroimaging methods and analytics have been developed to characterize structural connectivity of the brain by means of white matter fiber tracking using DWI [54]. These approaches are clinically significant in evaluating and treating network-wide diseases including affective disorders where white matter hubs are the primary neuromodulation targets [3], [20], [59], [60]. However, diffusion data is burdened with (1) risks of low signal-to-noise ratio related to patient movement during long acquisition sequences and (2) sampling volumes of multiple cubic millimeters which span many populations of neurons and axons. Error in the estimated direction of diffusion will accumulate across mixed axon populations within a voxel, especially when calculating streamlines between distant brain regions or smaller fiber tracts. The ‘streamlines’ used in tractography are a computational construct and cannot perfectly represent the degree of underlying white matter connectivity. Further, DWI isolates organized fiber bundles but cannot identify precise innervation points at the termini of specific fibers. Additionally,

the probabilistic tractography method has an intrinsic limitation of the producing false positive tracts that are not related to anatomical structures [31]. Despite these drawbacks, diffusion MRI remains one of the only techniques available for noninvasively assessing in vivo structural connectivity in humans, and as such is becoming relied upon for planning neurosurgical interventions.

Integration of data across multiple modalities can help characterize connectivity across the networks of interest in affective disorders, and in the case of single-pulse evoked potentials, the strengths of one method overlap with the weaknesses of the other. Evoked potentials can be elicited by single-pulse intracranial stimulation [29], [38], [61]–[63] where stimulation-driven events generate evoked responses, providing a mapping of the mechanistic connections between brain regions via causality. Evoked potentials primarily reflect aggregated synaptic activity across populations of neuronal cell bodies and dendrites, located in the gray matter and unmeasurable by diffusion-weighted imaging. However, these methods cannot independently ascertain the white matter pathway taken between stimulation and recording sites. This leads to challenges in identifying white matter pathways responsible for transmission of gray-matter initiated stimulation pulses. The stimulation method used in our experiment tethers electrical stimulation fields to a compatible structural quantity, the white matter fiber tract, and thus couples the DWI imaging to the stimulation-based effective connectivity network.

The current study suggests there may be substantial variability in which tracks are most amenable to fiber tracking and therefore most suitable for use in neurosurgical targeting. Tracks with poor concordance between fiber tracking and evoked potentials may indicate areas in which the tractography approaches incompletely characterize connectivity, suggesting the use of a secondary method for targeting, such as temporary micro-electrode recording or scalp electrophysiological methods to confirm implant targets are modulating distant regions appropriately.

Limitations and future directions:

Calculating streamlines and fiber tracks from DWI provides an approximate measure of white matter integrity and connectivity between a seed and a target volume in the brain. By contrast, evoked potentials are measurable almost exclusively in the gray matter as a phenomenon arising from concerted firing of assemblies of cell bodies and dendrites in the gray matter. To interlace these two modalities, the size of streamline calculation target masks centered on each sEEG contact was dilated enough to associate nearby white matter streamlines with gray matter contacts recording neural activity. A sufficient size for these sEEG masks was determined using ROC analysis (Figure S1). In this study, mask sizes were set globally across sEEG contacts for the calculation of intersecting streamlines without adjustment for (1) the percentage of white/gray matter contained within each mask, (2) the probability that the white/gray matter within a mask was connected, or (3) the anatomy surrounding each sEEG contact. Improving the efficiency of the mask creation could improve concordance between the two modalities.

Our analysis focused on treating evoked responses as a dichotomous variable. Furthermore, early responses (<10ms) after stimulation are possible and can provide valuable insights into

the circuitry invoked through stimulation [64], [65] but was not considered in our analysis as any signal was potentially overpowered by stimulation artifact returning to baseline. Evoked responses contain substantially more information in the produced waveform such as amplitudes and peak latencies, which could further elucidate the relationship with tractography. However, much of the single-pulse electrical stimulation literature is from ECoG recordings with subdural electrodes. Because of differing geometry, cylindrical sEEG contacts may include signal contributions from multiple nearby sources resulting in a mixed evoked response, complicating the interpretation of ERP waveform characteristics. Hence, techniques for identifying specific waveforms such as the N1/N2 found in Matsumoto et. al. [29] need further refinement prior to utilization in sEEG recorded ERPs. For the interested reader, we've provided an in-depth 3-dimensional visualization [66] of defined ROIs on a glass brain in Figure S2 with an exemplar set of stimulation evoked waveforms from patient A in Figure S5.

As a function of the parent study (UH3-NS103549), sEEG recording electrodes were placed prospectively within depression-related networks. The locations for sEEG leads were defined by prior tractography studies demonstrating their importance in treatment response [20], [67]. Further studies should ascertain whether structures outside of those implicated in depression show similar relationships between tractography and evoked responses. Furthermore, both DWI and evoked potentials reveal notably greater bilateral connectivity emanating from SCC fiber tracts compared to VCVS which showed primarily ipsilateral connectivity. However, the limitation of sEEG recording locations included in the current study does not allow us to determine if one stimulation target has greater connectivity overall. Future studies may further elucidate the differences in innervation patterns between the two targets by using more uniform sampling across both targets.

Lastly, the current study is limited by its sample size. Larger patient samples are also needed to provide the statistical power to consider the temporal component of the evoked potential response, in particular the latency of responses to indicate monosynaptic vs. polysynaptic transmission. It is possible that considering these elements of the evoked potential response may inform the degree to which DBS modulates structures directly or indirectly to exert its therapeutic effect.

Conclusion

This study found significant similarity between DWI-predicted structural connectivity and effective connectivity emerging from single-pulse evoked potentials. The relationship between these two measures is statistically robust, though there are clear areas of differentiation. The field of brain stimulation has increasingly relied on tractography to understand evoked effects of white matter stimulation approaches; the current data serve to temper that reliance and demonstrate the necessity of leveraging other approaches (electrophysiological and histological) to understand the circuit-wide effects of neuromodulation more deeply, especially to white matter targets. Thus, DTI and evoked potentials together may provide a holistic understanding of brain connectivity, further advancing the field of human brain mapping and neurosurgical white matter targeting.

Supplementary Material

Refer to Web version on PubMed Central for supplementary material.

Funding Sources:

KRB & BAM supported by NIH K01 MH103549, NIH R01 MH127006 and NIH R21 NS104953, CCM & AMN supported by NIH R01 NS105690, NP supported by NIH R01 NS097782, NIH UH3 NS113661, ET supported by NIH UH3 NS113661, NIH R01MH121089. MER supported by the Core for Advanced MRI (CAMRI) at Baylor College of Medicine and NIH R01 MH127006. SAS supported by McNair Foundation, Dana Foundation and NIH R01 MH127006. All authors supported by UH3 NS103549.

Special Thanks:

We are very grateful for the contributions of time and effort of our patients, the support of the Baylor St. Luke's Medical Center hospital staff including Katrina Reichardt, and the funding bodies supporting our work. We would like to acknowledge the substantial efforts of John Magnotti, Steve Carcieri, Allen Stutes, and Elizabeth Vasconcellos.

References

[1]. Weiss D et al. , "Subthalamic stimulation modulates cortical motor network activity and synchronization in Parkinson's disease," Brain, vol. 138, no. 3, pp. 679–693, 2015, doi: 10.1093/brain/awu380. [PubMed: 25558877]

[2]. Lujan JL et al. , "Tractography-activation models applied to subcallosal cingulate deep brain stimulation.," Brain Stimul, vol. 6, no. 5, pp. 737–739, Sep. 2013, doi: 10.1016/j.brs.2013.03.008. [PubMed: 23602025]

[3]. Riva-Posse P et al. , "Defining critical white matter pathways mediating successful subcallosal cingulate deep brain stimulation for treatment-resistant depression.," Biol. Psychiatry, vol. 76, no. 12, pp. 963–969, Dec. 2014, doi: 10.1016/j.biopsych.2014.03.029. [PubMed: 24832866]

[4]. Bezchlibnyk YB, Cheng J, Bijanki KR, Mayberg HS, and Gross RE, Subgenual Cingulate Deep Brain Stimulation for Treatment-Resistant Depression, Second Edi. Elsevier Ltd, 2018.

[5]. Bartsch AJ, Biller A, and Homola GA, Presurgical Tractography Applications. 2013.

[6]. Mayberg HS et al. , "Deep brain stimulation for treatment-resistant depression.," Neuron, vol. 45, no. 5, pp. 651–660, Mar. 2005, doi: 10.1016/j.neuron.2005.02.014. [PubMed: 15748841]

[7]. Malone DAJ et al. , "Deep brain stimulation of the ventral capsule/ventral striatum for treatment-resistant depression.," Biol. Psychiatry, vol. 65, no. 4, pp. 267–275, Feb. 2009, doi: 10.1016/j.biopsych.2008.08.029. [PubMed: 18842257]

[8]. Holtzheimer PE 3rd and Mayberg HS, "Deep brain stimulation for treatment-resistant depression.," Am. J. Psychiatry, vol. 167, no. 12, pp. 1437–1444, Dec. 2010, doi: 10.1176/appi.ajp.2010.10010141. [PubMed: 21131410]

[9]. Bewernick BH et al. , "Nucleus Accumbens Deep Brain Stimulation Decreases Ratings of Depression and Anxiety in Treatment-Resistant Depression," Biol. Psychiatry, vol. 67, no. 2, pp. 110–116, Jan. 2010, doi: 10.1016/j.biopsych.2009.09.013. [PubMed: 19914605]

[10]. Puigdemont D et al. , "Deep brain stimulation of the subcallosal cingulate gyrus: Further evidence in treatment-resistant major depression," Int. J. Neuropsychopharmacol, vol. 15, no. 1, pp. 121–133, Feb. 2012, doi: 10.1017/S1461145711001088. [PubMed: 21777510]

[11]. Lozano AM et al. , "A multicenter pilot study of subcallosal cingulate area deep brain stimulation for treatment-resistant depression," J. Neurosurg. JNS, vol. 116, no. 2, pp. 315–322, 2012, doi: 10.3171/2011.10.JNS102122.

[12]. Holtzheimer PE et al. , "Subcallosal cingulate deep brain stimulation for treatment-resistant unipolar and bipolar depression.," Arch. Gen. Psychiatry, vol. 69, no. 2, pp. 150–158, Feb. 2012, doi: 10.1001/archgenpsychiatry.2011.1456. [PubMed: 22213770]

[13]. Dougherty DD et al. , "A Randomized Sham-Controlled Trial of Deep Brain Stimulation of the Ventral Capsule/Ventral Striatum for Chronic Treatment-Resistant Depression," Biol.

Psychiatry, vol. 78, no. 4, pp. 240–248, Aug. 2015, doi: 10.1016/j.biopsych.2014.11.023. [PubMed: 25726497]

[14]. Puigdemont D et al. , "A randomized double-blind crossover trial of deep brain stimulation of the subcallosal cingulate gyrus in patients with treatment-resistant depression: A pilot study of relapse prevention," J. Psychiatry Neurosci, vol. 40, no. 4, pp. 224–231, 2015, doi: 10.1503/jpn.130295. [PubMed: 25652752]

[15]. Bergfeld IO et al. , "Deep Brain Stimulation of the Ventral Anterior Limb of the Internal Capsule for Treatment-Resistant Depression: A Randomized Clinical Trial," JAMA Psychiatry, vol. 73, no. 5, pp. 456–464, 2016, doi: 10.1001/jamapsychiatry.2016.0152. [PubMed: 27049915]

[16]. Holtzheimer PE et al. , "Subcallosal cingulate deep brain stimulation for treatment-resistant depression: a multisite, randomised, sham-controlled trial," The Lancet Psychiatry, vol. 4, no. 11, pp. 839–849, 2017, doi: 10.1016/S2215-0366(17)30371-1. [PubMed: 28988904]

[17]. Merkl A et al. , "Deep brain stimulation of the subcallosal cingulate gyrus in patients with treatment-resistant depression: A double-blinded randomized controlled study and long-term follow-up in eight patients.," J. Affect. Disord, vol. 227, pp. 521–529, Feb. 2018, doi: 10.1016/j.jad.2017.11.024. [PubMed: 29161674]

[18]. Roet M, Boonstra J, Sahin E, Mulders AEP, Leentjens AFG, and Jahanshahi A, "Deep Brain Stimulation for Treatment-Resistant Depression: Towards a More Personalized Treatment Approach.," J. Clin. Med, vol. 9, no. 9, Aug. 2020, doi: 10.3390/jcm9092729.

[19]. Makris N et al. , "Variability and anatomical specificity of the orbitofrontothalamic fibers of passage in the ventral capsule/ventral striatum (VC/VS): precision care for patient-specific tractography-guided targeting of deep brain stimulation (DBS) in obsessive compulsiv," Brain Imaging Behav., vol. 10, no. 4, pp. 1054–1067, Dec. 2016, doi: 10.1007/s11682-015-9462-9. [PubMed: 26518214]

[20]. Riva-Posse P et al. , "A connectomic approach for subcallosal cingulate deep brain stimulation surgery: prospective targeting in treatment-resistant depression.," Mol. Psychiatry, vol. 23, no. 4, pp. 843–849, Apr. 2018, doi: 10.1038/mp.2017.59. [PubMed: 28397839]

[21]. Gutman DA, Holtzheimer PE, Behrens TEJ, Johansen-Berg H, and Mayberg HS, "A tractography analysis of two deep brain stimulation white matter targets for depression.," Biol. Psychiatry, vol. 65, no. 4, pp. 276–282, Feb. 2009, doi: 10.1016/j.biopsych.2008.09.021. [PubMed: 19013554]

[22]. Coenen VA et al. , "Tractographic description of major subcortical projection pathways passing the anterior limb of the internal capsule. Corticopetal organization of networks relevant for psychiatric disorders," NeuroImage Clin, vol. 25, p. 102165, 2020, doi: 10.1016/j.nicl.2020.102165.

[23]. Li N et al. , "A unified connectomic target for deep brain stimulation in obsessive-compulsive disorder," Nat. Commun, vol. 11, no. 1, p. 3364, 2020, doi: 10.1038/s41467-020-16734-3. [PubMed: 32620886]

[24]. Clark DL et al. , "Tract-based analysis of target engagement by subcallosal cingulate deep brain stimulation for treatment resistant depression," Brain Stimul, vol. 13, no. 4, pp. 1094–1101, 2020, doi: 10.1016/j.brs.2020.03.006. [PubMed: 32417668]

[25]. Haber SN, Yendiki A, and Jbabdi S, "Four Deep Brain Stimulation Targets for Obsessive-Compulsive Disorder: Are They Different?," Biol. Psychiatry, 2020, doi: 10.1016/j.biopsych.2020.06.031.

[26]. Pierpaoli C, Jezzard P, Basser PJ, Barnett A, and Di Chiro G, "Diffusion tensor MR imaging of the human brain.," Radiology, vol. 201, no. 3, pp. 637–648, Dec. 1996, doi: 10.1148/radiology.201.3.8939209. [PubMed: 8939209]

[27]. Inoue T, Shimizu H, and Yoshimoto T, "Imaging the pyramidal tract in patients with brain tumors," Clin. Neurol. Neurosurg, vol. 101, no. 1, pp. 4–10, 1999, doi: 10.1016/S0303-8467(98)00069-9. [PubMed: 10350195]

[28]. Kennedy SH et al. , "Deep brain stimulation for treatment-resistant depression: Follow-up after 3 to 6 years," Am. J. Psychiatry, vol. 168, no. 5, pp. 502–510, 2011, doi: 10.1176/appi.ajp.2010.10081187. [PubMed: 21285143]

[29]. Matsumoto R, Nair DR, LaPresto E, Bingaman W, Shibasaki H, and Lüders HO, "Functional connectivity in human cortical motor system: a cortico-cortical evoked potential study.," Brain, vol. 130, no. Pt 1, pp. 181–197, Jan. 2007, doi: 10.1093/brain/awl257. [PubMed: 17046857]

[30]. Jeurissen B, Descoteaux M, Mori S, and Leemans A, "Diffusion MRI fiber tractography of the brain.," NMR Biomed, vol. 32, no. 4, p. e3785, Apr. 2019, doi: 10.1002/nbm.3785. [PubMed: 28945294]

[31]. Maier-Hein KH et al. , "The challenge of mapping the human connectome based on diffusion tractography," Nat. Commun, vol. 8, no. 1, p. 1349, 2017, doi: 10.1038/s41467-017-01285-x. [PubMed: 29116093]

[32]. Yeh C-H, Jones DK, Liang X, Descoteaux M, and Connelly A, "Mapping Structural Connectivity Using Diffusion MRI: Challenges and Opportunities," J. Magn. Reson. Imaging, vol. n/a, no. n/a, doi: 10.1002/jmri.27188.

[33]. Girard G et al. , "On the cortical connectivity in the macaque brain: A comparison of diffusion tractography and histological tracing data.," Neuroimage, vol. 221, p. 117201, Nov. 2020, doi: 10.1016/j.neuroimage.2020.117201. [PubMed: 32739552]

[34]. Donahue CJ et al. , "Using Diffusion Tractography to Predict Cortical Connection Strength and Distance: A Quantitative Comparison with Tracers in the Monkey.," J. Neurosci, vol. 36, no. 25, pp. 6758–6770, Jun. 2016, doi: 10.1523/JNEUROSCI.0493-16.2016. [PubMed: 27335406]

[35]. Choi EY, Ding S-L, and Haber SN, "Combinatorial Inputs to the Ventral Striatum from the Temporal Cortex, Frontal Cortex, and Amygdala: Implications for Segmenting the Striatum.," eNeuro, vol. 4, no. 6, 2017, doi: 10.1523/ENEURO.0392-17.2017.

[36]. Elias WJ, Zheng ZA, Domer P, Quigg M, and Pouratian N, "Validation of connectivity-based thalamic segmentation with direct electrophysiologic recordings from human sensory thalamus," Neuroimage, vol. 59, no. 3, pp. 2025–2034, Feb. 2012, doi: 10.1016/j.neuroimage.2011.10.049. [PubMed: 22036683]

[37]. Kang G and Lowery M, "Effects of antidromic and orthodromic activation of STN afferent axons during DBS in Parkinson's disease: a simulation study," Front. Comput. Neurosci, vol. 8, p. 32, 2014, doi: 10.3389/fncom.2014.00032. [PubMed: 24678296]

[38]. Borchers S, Himmelbach M, Logothetis N, and Karnath H-O, "Direct electrical stimulation of human cortex — the gold standard for mapping brain functions?," Nat. Rev. Neurosci, vol. 13, no. 1, pp. 63–70, 2012, doi: 10.1038/nrn3140.

[39]. Allawala A et al. , "A Novel Framework for Network-Targeted Neuropsychiatric Deep Brain Stimulation," Neurosurgery, Apr. 2021, doi: 10.1093/neuros/nyab112.

[40]. Drobisz D and Damborská A, "Deep brain stimulation targets for treating depression," Behav. Brain Res, vol. 359, no. May 2018, pp. 266–273, 2019, doi: 10.1016/j.bbr.2018.11.004. [PubMed: 30414974]

[41]. Williams LM, "Precision psychiatry: a neural circuit taxonomy for depression and anxiety.," The lancet. Psychiatry, vol. 3, no. 5, pp. 472–480, May 2016, doi: 10.1016/S2215-0366(15)00579-9. [PubMed: 27150382]

[42]. Drysdale AT et al. , "Resting-state connectivity biomarkers define neurophysiological subtypes of depression," Nat. Med, vol. 23, no. 1, pp. 28–38, 2017, doi: 10.1038/nm.4246. [PubMed: 27918562]

[43]. Fischl B, "FreeSurfer.," Neuroimage, vol. 62, no. 2, pp. 774–781, Aug. 2012, doi: 10.1016/j.neuroimage.2012.01.021. [PubMed: 22248573]

[44]. Jenkinson M and Smith S, "A global optimisation method for robust affine registration of brain images.," Med. Image Anal, vol. 5, no. 2, pp. 143–156, Jun. 2001, doi: 10.1016/s1361-8415(01)00036-6. [PubMed: 11516708]

[45]. Jenkinson M, Bannister P, Brady M, and Smith S, "Improved Optimization for the Robust and Accurate Linear Registration and Motion Correction of Brain Images," Neuroimage, vol. 17, no. 2, pp. 825–841, Oct. 2002, doi: 10.1006/nimg.2002.1132. [PubMed: 12377157]

[46]. Joshi A et al. , "Unified framework for development, deployment and robust testing of neuroimaging algorithms.," Neuroinformatics, vol. 9, no. 1, pp. 69–84, Mar. 2011, doi: 10.1007/s12021-010-9092-8. [PubMed: 21249532]

[47]. Magnotti JF, Wang Z, and Beauchamp MS, “RAVE: Comprehensive open-source software for reproducible analysis and visualization of intracranial EEG data,” Neuroimage, vol. 223, p. 117341, 2020, doi: 10.1016/j.neuroimage.2020.117341.

[48]. McIntyre CC, Richardson AG, and Grill WM, “Modeling the Excitability of Mammalian Nerve Fibers: Influence of Afterpotentials on the Recovery Cycle,” J. Neurophysiol, vol. 87, no. 2, pp. 995–1006, 2002, doi: 10.1152/jn.00353.2001. [PubMed: 11826063]

[49]. Andersson JLR, Skare S, and Ashburner J, “How to correct susceptibility distortions in spin-echo echo-planar images: Application to diffusion tensor imaging,” Neuroimage, vol. 20, no. 2, pp. 870–888, 2003, doi: 10.1016/S1053-8119(03)00336-7. [PubMed: 14568458]

[50]. Andersson JLR, Graham MS, Zsoldos E, and Sotiropoulos SN, “Incorporating outlier detection and replacement into a non-parametric framework for movement and distortion correction of diffusion MR images,” Neuroimage, vol. 141, pp. 556–572, 2016, doi: 10.1016/j.neuroimage.2016.06.058. [PubMed: 27393418]

[51]. Behrens TEJ et al. , “Characterization and Propagation of Uncertainty in Diffusion-Weighted MR Imaging,” Magn. Reson. Med, vol. 50, no. 5, pp. 1077–1088, 2003, doi: 10.1002/mrm.10609. [PubMed: 14587019]

[52]. Smith SM, “Fast robust automated brain extraction,” Hum. Brain Mapp, vol. 17, no. 3, pp. 143–155, 2002, doi: 10.1002/hbm.10062. [PubMed: 12391568]

[53]. Zhang Y, Brady M, and Smith S, “Segmentation of brain MR images through a hidden Markov random field model and the expectation-maximization algorithm,” IEEE Trans. Med. Imaging, vol. 20, no. 1, pp. 45–57, 2001, doi: 10.1109/42.906424. [PubMed: 11293691]

[54]. Behrens TEJ, Berg HJ, Jbabdi S, Rushworth MFS, and Woolrich MW, “Probabilistic diffusion tractography with multiple fibre orientations: What can we gain?,” Neuroimage, vol. 34, no. 1, pp. 144–155, 2007, doi: 10.1016/j.neuroimage.2006.09.018. [PubMed: 17070705]

[55]. Li G et al. , “Optimal referencing for stereo-electroencephalographic (SEEG) recordings,” Neuroimage, vol. 183, pp. 327–335, Dec. 2018, doi: 10.1016/j.neuroimage.2018.08.020. [PubMed: 30121338]

[56]. Robin X et al. , “pROC: an open-source package for R and S+ to analyze and compare ROC curves,” BMC Bioinformatics, vol. 12, no. 1, p. 77, 2011, doi: 10.1186/1471-2105-12-77. [PubMed: 21414208]

[57]. DeLong ER, DeLong DM, and Clarke-Pearson DL, “Comparing the areas under two or more correlated receiver operating characteristic curves: a nonparametric approach.,” Biometrics, vol. 44, no. 3, pp. 837–845, Sep. 1988. [PubMed: 3203132]

[58]. V North B, Curtis D, and Sham PC, “A note on the calculation of empirical P values from Monte Carlo procedures,” Am. J. Hum. Genet, vol. 71, no. 2, pp. 439–441, Aug. 2002, doi: 10.1086/341527. [PubMed: 12111669]

[59]. Coenen VA, Panksepp J, Hurwitz TA, Urbach H, and Mädler B, “Human medial forebrain bundle (MFB) and anterior thalamic radiation (ATR): imaging of two major subcortical pathways and the dynamic balance of opposite affects in understanding depression.,” J. Neuropsychiatry Clin. Neurosci, vol. 24, no. 2, pp. 223–236, 2012, doi: 10.1176/appi.neuropsych.11080180. [PubMed: 22772671]

[60]. Tyagi H et al. , “A Randomized Trial Directly Comparing Ventral Capsule and Anteromedial Subthalamic Nucleus Stimulation in Obsessive-Compulsive Disorder: Clinical and Imaging Evidence for Dissociable Effects,” Biol. Psychiatry, vol. 85, no. 9, pp. 726–734, May 2019, doi: 10.1016/j.biopsych.2019.01.017. [PubMed: 30853111]

[61]. Waters AC et al. , “Test–retest reliability of a stimulation-locked evoked response to deep brain stimulation in subcallosal cingulate for treatment resistant depression,” Hum. Brain Mapp, vol. 39, no. 12, pp. 4844–4856, 2018, doi: 10.1002/hbm.24327. [PubMed: 30120851]

[62]. Waters AC, Song JE, Luu P, and Tucker DM, “The Importance of Single Trials: Temporal and Spatial Resolution in Event-Related Potential Research,” Dev. Neuropsychol, vol. 37, no. 6, pp. 545–558, 2012, doi: 10.1080/87565641.2012.674994. [PubMed: 22889344]

[63]. Shine JM et al. , “Distinct Patterns of Temporal and Directional Connectivity among Intrinsic Networks in the Human Brain.,” J. Neurosci, vol. 37, no. 40, pp. 9667–9674, Oct. 2017, doi: 10.1523/JNEUROSCI.1574-17.2017. [PubMed: 28893929]

[64]. Miocinovic S et al. , “Cortical Potentials Evoked by Subthalamic Stimulation Demonstrate a Short Latency Hyperdirect Pathway in Humans,” J. Neurosci, vol. 38, no. 43, pp. 9129–9141, 2018, doi: 10.1523/JNEUROSCI.1327-18.2018. [PubMed: 30201770]

[65]. Schmidt SL, Brocker DT, Swan BD, Turner DA, and Grill WM, “Evoked potentials reveal neural circuits engaged by human deep brain stimulation,” Brain Stimul, vol. 13, no. 6, pp. 1706–1718, 2020, doi: 10.1016/j.brs.2020.09.028. [PubMed: 33035726]

[66]. Felsenstein O et al. , “Multi-Modal Neuroimaging Analysis and Visualization Tool (MMVT),” arXiv:1912.10079 [q-bio], Sep. 2019, [Online]. Available: http://arxiv.org/abs/1912.10079.

[67]. Tsolaki E, Espinoza R, and Pouratian N, “Using probabilistic tractography to target the subcallosal cingulate cortex in patients with treatment resistant depression.,” Psychiatry Res. Neuroimaging, vol. 261, pp. 72–74, Mar. 2017, doi: 10.1016/j.pscychresns.2017.01.006. [PubMed: 28142056]

Highlights

- Patients with TRD underwent a clinical trial implanting DBS and temporary sEEG electrodes.
- During sEEG, a single-pulse stimulation experiment examined network connectivity.
- Single-pulse evoked potentials were directly compared with patient-specific DTI in 2 patients.
- Several regions showed similarity between structural and electrophysiological connectivity.
- Areas of incongruity between DTI and electrophysiology suggest areas for further evaluation.

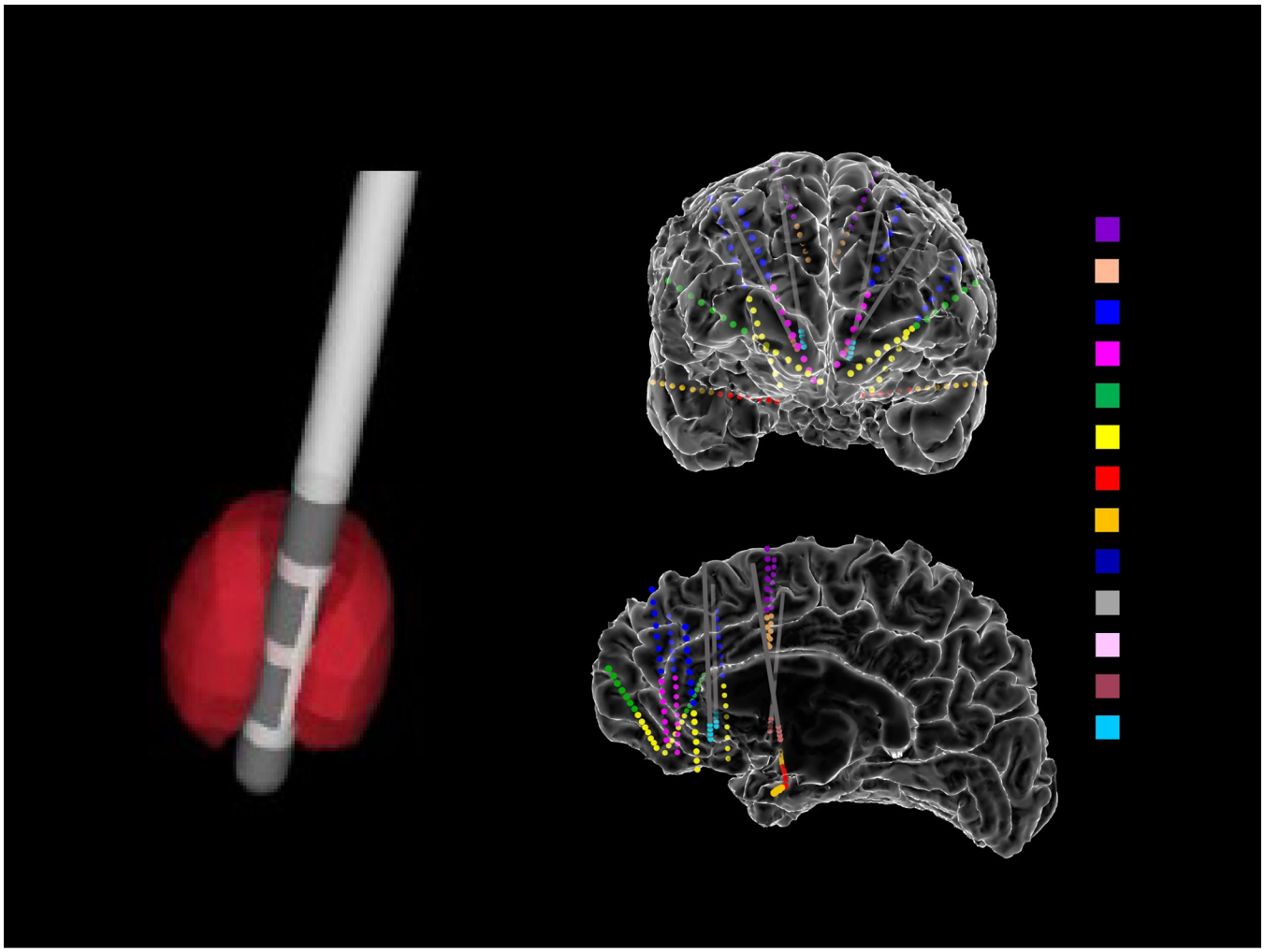

Figure 1: Examples of DBS Lead and sEEG implantation strategy.

(A) Computer rendered close-up of the Boston Scientific Cartesia DBS lead. The red volume represents an example stimulation field model produced by the lead during stimulation of stacked monopolar contacts. (B) Placement of sEEG electrodes in Patient A as presented on a glass brain color-coded regions of interest denoted to the right. See supplementary figure S2 for sEEG electrode placement for both patients.

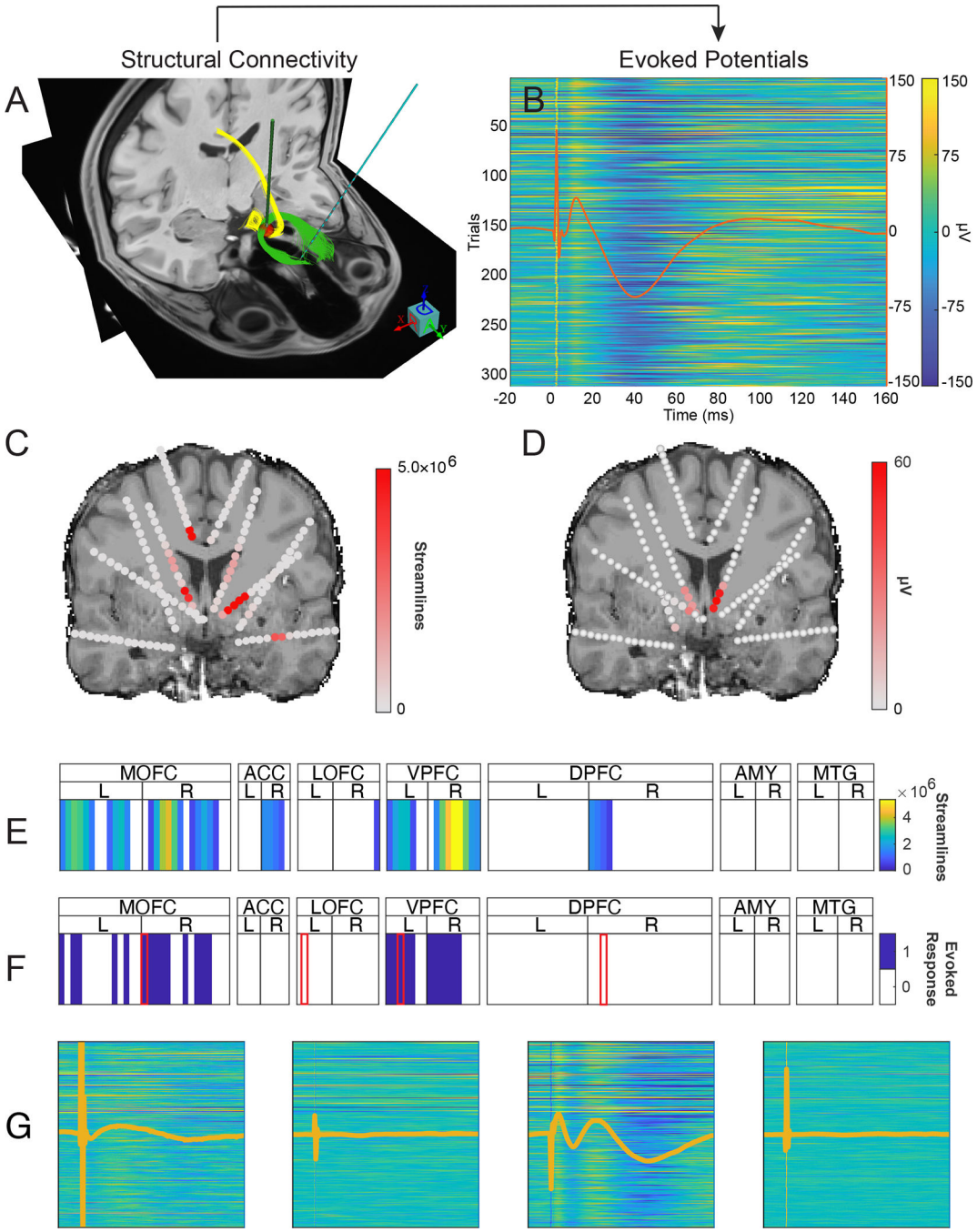

Figure 2: Example of evoked potential and streamline analysis for a single stimulation volume.

Two treatment-resistant depression patients underwent neurosurgical treatment involving DBS. We compare tractography from pre-surgical MRI to post-surgical in vivo recordings. (A) Given the stimulation volume of interest as Right SCC monopolar stacked segmented contacts 4 and 7, (red sphere) the diffusion tractography to the whole brain is performed and intersection with the sEEG contact of interest (Left OFC contact 3) is calculated. (B) 315 single-pulse stimulation trials are applied to the Right SCC monopolar contacts 4 and 7, and evoked potentials are measured at the same sEEG contact as measured

via streamlines in Panel A. (C&E) The process is repeated to calculate the number of streamlines intersecting all sEEG contacts in the brain. (D&F) Evoked potentials arising from RSCC 4–7 stimulation are calculated from all sEEG contacts. Warmer colors indicated greater numbers of streamlines (Panel C) and higher voltage evoked potentials averaged across 315 trials (Panel D). These data are reduced to a single row, with white cells represent targets with less than 500,000 streamlines (Panel E) and contacts where no evoked potential waveform was detected (Panel F). (G) Four exemplar traces derived from single-pulse stimulation. Traces have the same scaling as (B) and are associated from left-to-right with the contacts indicated by a red border in Panel F.

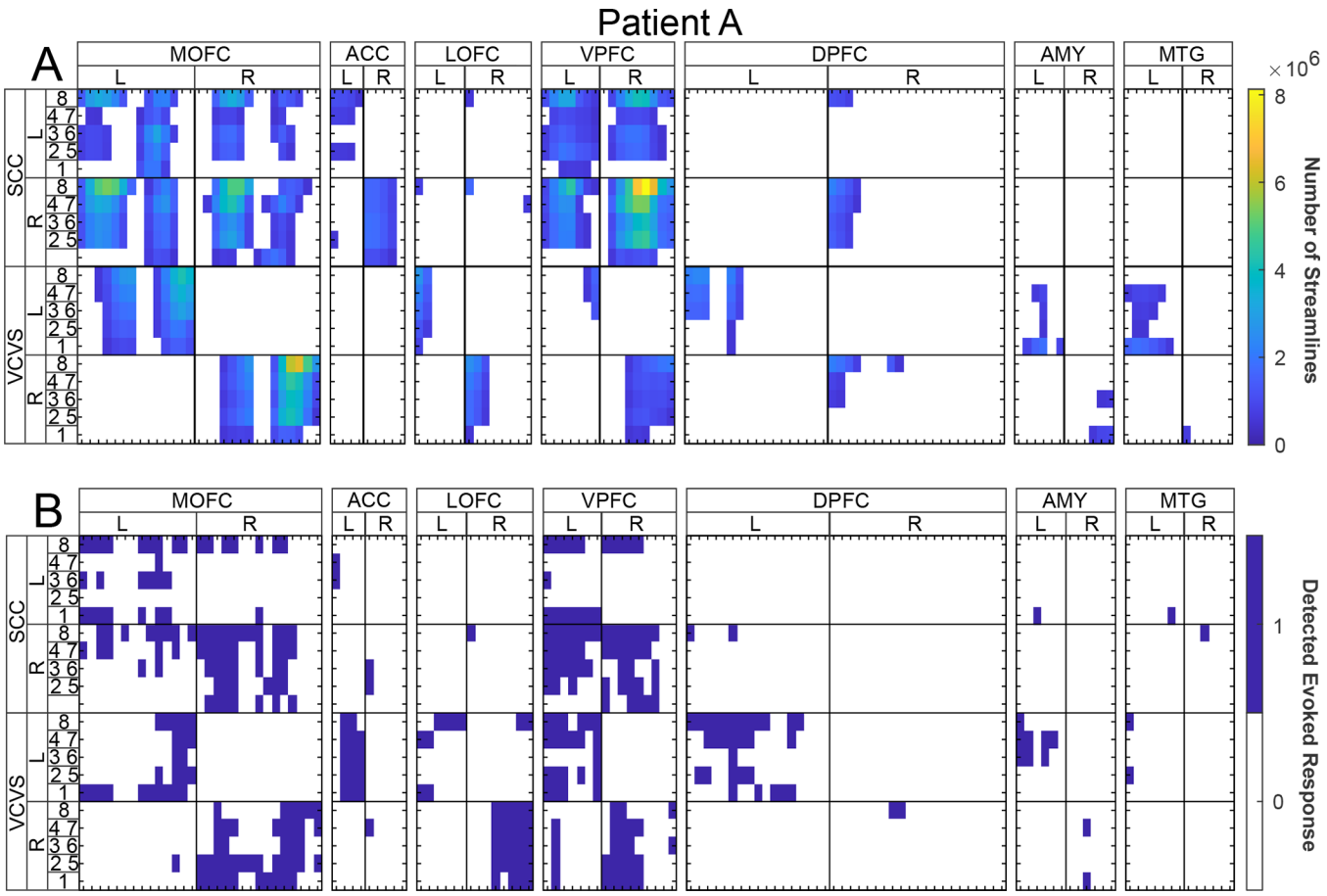

Figure 3: Patient A direct comparison between streamlines and evoked potentials elicited by stimulation contact configurations at sEEG contact regions of interest.

(A) Columns separated by tick marks across the X-axis indicate individual sEEG electrode contacts – for specific anatomical information see Supplemental Material S2, S3, and S4. Warmer colors indicate a greater number of streamlines predicted to reach each sEEG recording contact (X-axis) based on the physical shape of the stimulation field models for each stimulation configuration (Y-axis). Streamlines are calculated to intersect a 10mm spherical mask surrounding the given sEEG contact. White cells represent regions with less than 500,000 streamline intersections. (B) Evoked potentials generated by each stimulation configuration (Y-axis), in terms of average μV magnitude recorded at each of the sEEG contacts (X-axis). White cells represent sEEG contacts where no evoked potential was detected from the given stimulation experiment. For each panel, a given column measures the effect of the given measurement for a single sEEG contact as specified by the section heading. Anatomical regions of interest are used to group sEEG contacts, with the leftmost cell in a set representing the contact most distal to the brain surface and rightmost cell of the set being the most proximal to the brain surface. Rows for each figure represent the contact(s) stimulated from the given DBS lead with stimulation contacts on the same electrode situated as adjacent columns, left and right hemisphere electrodes set on the left and right sides of the heatmaps, respectively. Cooler colors represent smaller values.

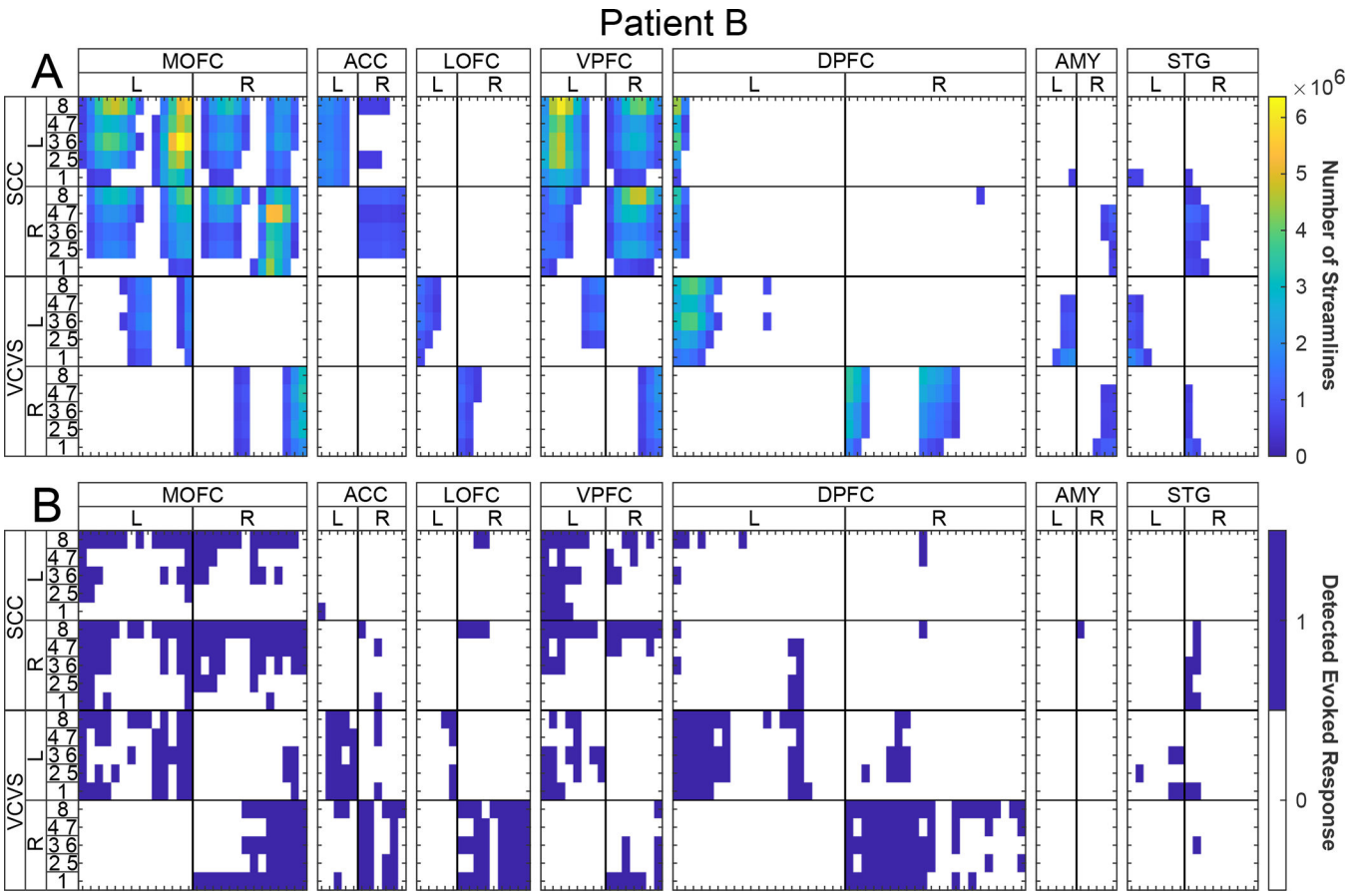

Figure 4: Patient B direct comparison between streamlines and evoked potentials elicited by stimulation contact configurations at sEEG contact regions of interest.

(A) Columns separated by tick marks across the X-axis indicate individual sEEG electrode contacts – for specific anatomical information see Supplemental Material S2, S3, and S4. Warmer colors indicate a greater number of streamlines predicted to reach each sEEG recording contact (X-axis) based on the physical shape of the stimulation field models for each stimulation configuration (Y-axis). Streamlines are calculated to intersect a 10mm spherical mask surrounding the given sEEG contact. White cells represent regions with less than 500,000 streamline intersections. (B) Evoked potentials generated by each stimulation configuration (Y-axis), in terms of average μV magnitude recorded at each of the sEEG contacts (X-axis). White cells represent sEEG contacts where no evoked potential was detected from the given stimulation experiment. For each panel, a given column measures the effect of the given measurement for a single sEEG contact as specified by the section heading. Anatomical regions of interest are used to group sEEG contacts, with the leftmost cell in a set representing the contact most distal to the brain surface and rightmost cell of the set being the most proximal to the brain surface. Rows for each figure represent the contact(s) stimulated from the given DBS lead with stimulation contacts on the same electrode situated as adjacent columns, left and right hemisphere electrodes set on the left and right sides of the heatmaps, respectively. Cooler colors represent smaller values.

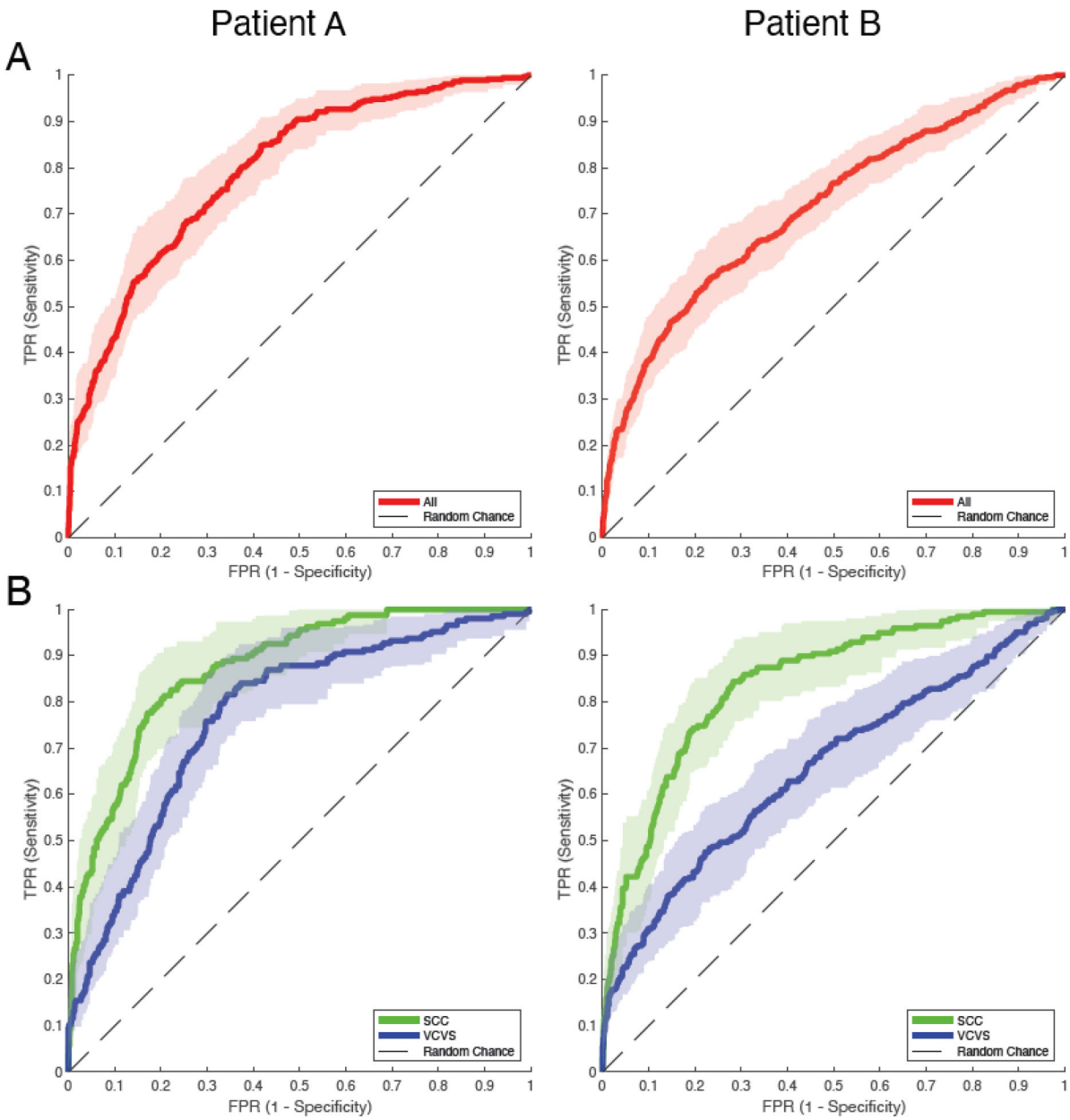

Figure 5: Receiver operating characteristic curves quantifying the relationship between evoked potentials and streamlines across all trials, stimulation configurations, and recording positions.

(A) ROC curves of evoked potential occurrences versus the number of streamlines for Patients A and B. Red lines represent the original ROC for all reported stimulation experiments with shaded regions representing confidence intervals for each True Positive Rate (TPR) with respect to each False Positive Rate (FPR). (B) ROC curves of evoked potential occurrences versus the number of streamlines for Patients A and B with respect to the DBS targets. Blue lines represent the ROC for the VCVS targets and green lines represent the ROC for the SCC targets. Shaded regions are the 95% confidence intervals for each ROC taken in the same manner as (A).